Approaching Maximal Precision of Hong-Ou-Mandel Interferometry with Nonperfect Visibility

O. Meskine,[1,*] E. Descamps,[1,2,*] A. Keller,[1,3] A. Lemaître,[4] F. Baboux,[1] S. Ducci,[1,†] and P. Milman[1,‡]
[1]Laboratoire Matériaux et Phénomènes Quantiques, Université Paris Cité, CNRS UMR 7162, 75013 Paris, France
[2]Département de Physique de l'Ecole Normale Supérieure - PSL, 45 rue d'Ulm, 75230 Paris Cedex 05, France
[3]Department de Physique, Université Paris-Saclay, 91405 Orsay Cedex, France
[4]Univ. Paris-Saclay, CNRS, Centre de Nanosciences et de Nanotechnologies, 91120 Palaiseau, France

(Received 20 September 2023; accepted 8 April 2024; published 7 May 2024)

In quantum mechanics, the precision achieved in parameter estimation using a quantum state as a probe is determined by the measurement strategy employed. The quantum limit of precision is bounded by a value set by the state and its dynamics. Theoretical results have revealed that in interference measurements with two possible outcomes, this limit can be reached under ideal conditions of perfect visibility and zero losses. However, in practice, these conditions cannot be achieved, so precision *never* reaches the quantum limit. But how do experimental setups approach precision limits under realistic circumstances? In this Letter, we provide a model for precision limits in two-photon Hong-Ou-Mandel interferometry using coincidence statistics for nonperfect visibility and temporally unresolved measurements. We show that the scaling of precision with visibility depends on the effective area in time-frequency phase space occupied by the state used as a probe, and we find that an optimal scaling exists. We demonstrate our results experimentally for different states in a setup where the visibility can be controlled and reaches up to 99.5%. In the optimal scenario, a ratio of 0.97 is observed between the experimental precision and the quantum limit, establishing a new benchmark in the field.

DOI: 10.1103/PhysRevLett.132.193603

The Hong-Ou-Mandel (HOM) interferometer is often used to demonstrate the phenomenon of bunching of two identical, independent bosonic quantum particles, such as single photons [1] (see Fig. 1). In this setup, photons are made to interfere on a balanced beam splitter (BS) and their detection in coincidence at the output indicates whether they have bunched or not. To control the distinguishability of the two paths of the interferometer, a time delay can be introduced for one of the input photons, consequently changing the coincidence detection probability. Despite its seemingly straightforward operating principles, the HOM interferometer has found diverse applications beyond its original scope [2]: the coincidence detection signal at the BS output has been demonstrated to serve as an entanglement witness [3–5], to provide phase space information about the spectral function [6–8], and to enable the simulation of different quantum exchange statistics [9,10], among other applications [11–13]. In particular, the HOM interferometer is a valuable apparatus for quantum parameter estimation both in the time unresolved [14–20] and time resolved measurement regimes [21]: its low-intensity regime opens the possibility of applying the tools of quantum metrology to small and fragile probes, such as biological ones [22]; since the HOM effect is based on two-photon interference, it is robust against background noise, group velocity dispersion [23], and phase perturbations [24]. Last but not least, theoretical and experimental results indicate that it can arbitrarily approach the quantum precision limit for time delay (or path difference) estimation [14,15,18,20,21]. However, in spite of the recent experiments reaching up to attosecond precision on time delay estimations [16–18,20,25], the mechanisms determining the limits and limitations of different quantum states for time measurement precision using the HOM with respect to the maximal achievable precision are unknown under realistic conditions of nonperfect visibility. In particular, such limitations depend on the adopted measurement strategy. In this Letter we will concentrate on the time unresolved measurement regime with unresolved photon number detection where, if losses are ignored, photons

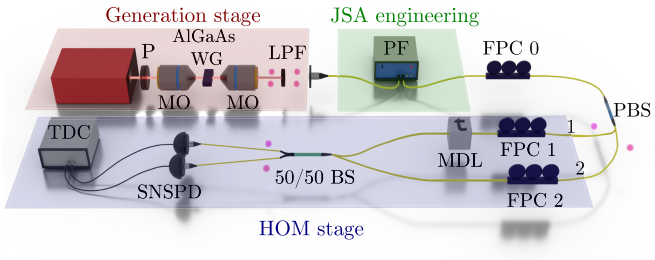

FIG. 1. Experimental setup for investigating the metrological performance of the Hong-Ou-Mandel (HOM) experiment, showing the generation, joint spectral amplitude (JSA) engineering, and HOM interferometer stages.

either bunch or antibunch at each run of the experiment, leading to a two possible outcomes experiment [26]. A curious result observed not only for HOM interferometers but also for any parameter estimation protocol based on dichotomic measurements (see also [33,34], for instance) concerns the behavior of precision with the visibility V at the point where, in the ideal case, the former is expected to saturate the quantum limit. For instance in the HOM setup, if $V = 1$, one can attain the quantum precision limit at zero delay, where photons either perfectly bunch or antibunch. Nevertheless, in the experimentally realistic case where the visibility $V < 1$, total bunching or antibunching is no longer observed and precision drops down to zero at this time delay. A way to circumvent this in the context of a Mach-Zender interferometer was studied in [27] using a mode-engineering-based strategy. As for the HOM experiment, for finite visibility, the quantum precision limit can only be approached, and the maximal attainable precision will occur for a finite delay between photons, as discussed later in this Letter. However, it is not clear if and how the maximal achievable precision depends on the probe's state spectral function in a HOM experiment for a given visibility [15,17–19].

In this Letter, we provide a theoretical model and its experimental demonstration explaining both qualitatively and quantitatively the performance of the HOM experiment as a quantum metrological tool, as a function of the input state and visibility. For such, we have exactly theoretically predicted and experimentally confirmed the wave function dependency of the scaling of the maximal precision with the visibility for different wave functions and interpreted our results in terms of phase space properties. For some configurations, we reach the highest ratio between the achieved precision and the maximum possible one to date, thereby setting a new benchmark in this field.

In a typical metrological protocol, a probe is prepared in an initial state, and undergoes a dynamical evolution depending on a parameter to be estimated, θ. The probe is measured providing an outcome k, which is used to estimate θ. By associating the function $p_k(\theta)$ to the probability of obtaining an outcome k, the precision on the estimation of θ is bounded by the relation $\delta\theta \geq 1/\sqrt{\nu F(\theta)}$, where $F(\theta) = \sum_k (1/p_k(\theta))[\partial p_k(\theta)/\partial\theta]^2$ is the Fisher information (FI) and ν is the number of repetitions of the experiment. When using quantum mechanical resources—as individual photons, which is the case in a HOM experiment—one can define the quantum Fisher information (QFI) by using a quantum state as a probe [35]. The probe's evolution depends on the parameter θ, and for pure states and unitary evolutions, this dependency can be expressed as $|\psi(\theta)\rangle = e^{i\hat{H}\theta}|\psi\rangle$, where $\hat{H}$ is the Hamiltonian generating the dynamical evolution. Precision is thus limited by the relation $\delta\theta \geq 1/\sqrt{\nu\mathcal{F}}$, where $\mathcal{F}$ is the QFI, obtained by maximizing $F(\theta)$ over all possible measurements on $|\psi(\theta)\rangle$. In the case discussed above, $\mathcal{F} = 4\Delta^2\hat{H}$, where the variance is taken with respect to the initial state $|\psi\rangle$ [36]. The bound $1/\sqrt{\nu\mathcal{F}}$ is called the "quantum Cramér-Rao bound" (QCR) [37], the quantum precision limit [38].

There is no general rule for finding an experimental measurement strategy where $F(\theta) = \mathcal{F}$, even though optimization procedures can be applied to particular states [39,40] and symmetry arguments can be evoked in specific situations [41,42], as in the HOM experiment [14,16]. As shown in the literature, time precision in HOM interferometry with perfect visibility can reach the QCR bound [15,16,18,20]. Consequently, several attempts have been made to reach this bound, obtaining astonishing precision on the estimation of time delays in HOM experiments [17–20]. To analyze these results, we consider as initial state (probe) a photon pair prepared in an arbitrary pure state that enters the two input arms 1,2 of a perfectly balanced BS,

$$|\psi\rangle = \int\int d\omega_1 d\omega_2 f(\omega_1,\omega_2)\hat{a}_1^\dagger(\omega_1)\hat{a}_2^\dagger(\omega_2)|0\rangle, \quad (1)$$

where $f(\omega_1,\omega_2)$ is the complex-valued normalized joint spectral amplitude (JSA). Before impinging the balanced BS, one of the photons in (1) is subjected to a time delay τ, the parameter to be estimated. This delay is described by a unitary evolution associated to the Hamiltonian $\hat{H} = \hbar\int d\omega\omega\hat{a}_1^\dagger(\omega)\hat{a}_1(\omega) = \hbar\hat{\omega}_1$ (we have supposed that arm 1 is delayed). State (1) becomes $|\psi(\tau)\rangle = e^{i\hat{H}\tau/\hbar}|\psi\rangle = \hat{U}|\psi\rangle$. After the BS, the probability of detecting both photons in coincidence $P_c(\tau) = \frac{1}{2}(1 - \langle\psi|\hat{U}^\dagger\hat{S}\,\hat{U}\,|\psi\rangle)$ [14], where $\hat{S}\hat{a}_1^\dagger(\omega_1)\hat{a}_2^\dagger(\omega_2)\hat{S}^\dagger = \hat{a}_1^\dagger(\omega_2)\hat{a}_2^\dagger(\omega_1)$ is a swap of spatial modes. $P_c(\tau)$ is typically directly obtained from the recorded experimental data. $P_a(\tau)$, the probability of anticoincidences, can either be inferred from direct detection [20] or using $P_a(\tau) = 1 - P_c(\tau)$ [43]. Finally, the QFI can be expressed as [26] $\mathcal{F} = 4\Delta^2\hat{\omega}_1$. For perfectly symmetric (S) [antisymmetric (AS)] states $|\psi\rangle_{\mathrm{S(AS)}}$ with respect to the exchange of spatial modes, $\hat{S}|\psi\rangle_{\mathrm{S(AS)}} = \pm|\psi\rangle_{\mathrm{S(AS)}}$ and $P_c(\tau = 0) = 0(1)$. Hence, the HOM has perfect visibility and the QFI can be reached.

The HOM experiment provides information about the collective variables $\omega_- = \omega_1 - \omega_2$ [16]. We will consider that the input photons of the interferometer are generated by spontaneous parametric down-conversion and that $f(\omega_1,\omega_2) = f_-(\omega_-)f_+(\omega_+)$ in (1), with $\omega_\pm = \omega_1 \pm \omega_2$. Functions f_- and f_+ are normalized functions related to the phase matching condition and to the energy conservation, respectively. The best configuration for metrology is the one where f_+ is a Dirac function centered on ω_p (the pump's frequency) and ω_+ is close to constant (strict energy conservation), maximizing the frequency correlation between photons [44,45]. Therefore, supposing that both photons have the same spectral

variance, $\mathcal{F}=4\Delta^2\omega_1=\Delta^2\omega_-$. In addition, $\langle\psi|\hat{U}^\dagger\hat{S}\,\hat{U}\,|\psi\rangle = \int d\omega_- e^{i\omega_-\tau} f_-(\omega_-)f_-^*(-\omega_-) = W(0,\tau)$. Here, $W(\mu,\tau)$ denotes the chronocyclic Wigner function associated with $f_-(\omega_-)$ on the time-frequency phase space (TFPS), specifically on the axis $\mu=0$ while τ, the time delay, is variable. Hence, μ is the phase space variable associated with ω_-. It was shown in [6] and experimentally validated in [7,8] that the HOM experiment directly measures the Wigner function points $W(0,\tau)$, i.e., along the axis $\mu=0$ of TFPS. Adopting this representation facilitates an intuitive understanding of the factors that dictate the limitations imposed by nonperfect visibility, which we study in the following.

To this aim, we model the dependency of $P_c(\tau)$ with the visibility V as [26]

$$P_c(\tau)=\frac{1}{2}-\frac{V}{2}W(0,\tau), \tag{2}$$

where $0\le V\le 1$ and $W(0,\tau)$ is the Wigner function of a perfectly symmetric state [46], so $W(0,0)=1$ and $P_c(0)=(1-V)/2$, defining the visibility. We are not considering explicitly the role of experimental noise or losses in the measurement, evolution, or preparation steps: they can either be included in the QFI, which is consequently modified, or in the state's purity [47,48]. Including noise in the state corresponds to considering a different (nonpure) state as a probe, so a different function $W(0,\tau)$. Thus, state noise or measurement losses have no incidence on the model (2), that remains valid. In addition, loss and visibility are independent quantities and even for pure states in a lossless configuration a nonunit visibility can be observed due to state preparation imperfections that cannot be circumvented [26]. Hence, we will focus exclusively on the visibility in the present work. Using (2), the FI at point τ is given by

$$F(V,\tau)=V^2\frac{[W'(0,\tau)]^2}{1-V^2W^2(0,\tau)}, \tag{3}$$

where $'$ denotes the time derivative. By defining $\max_\tau F(V,\tau)\overset{\text{def}}{=}\tilde{F}_V$, we obtain, for $V=1$ (perfectly S or AS states), $\tilde{F}_1=F(1,0)=\mathcal{F}$ [14,16,42]. This shows that the quantum precision limit can be achieved for perfect visibility. For $V\neq 1$ we can still compute $\tilde{F}_V$, which is obtained at a point $\tau=\tau_M\neq 0$. As a matter of fact, for $\tau=0$, the function $F(V,0)$, when considered as a function of V, exhibits a discontinuity at $V=1$: indeed, $F(V<1,0)=0$, while $F(1,0)=\tilde{F}_1=\mathcal{F}$, as previously shown. For $V<1$, the maximal values of $\tilde{F}_{V<1}$ satisfying $\tilde{F}_{V<1}=-W''(0,\tau_M)/W(0,\tau_M)$. Experimental investigations of these results were conducted in [17,19,20], and [33], but the overall behavior of the attainable values of $\tilde{F}_V$ and how their limitations and their scaling with visibility is related to the state's wave function remains unknown. We will now elucidate how $\tilde{F}_V$ approaches $\mathcal{F}$. Importantly, we find that this approach depends not only on the visibility but we also identify a relation with the effective phase space occupation of the state's Wigner function $W(\mu,\tau)$. Indeed, the scaling of $\tilde{F}_V$ with V is connected to how far the quantum state is from saturating the time-frequency Heisenberg uncertainty principle [49,50]. A first remark is that since $V\le 1$, Eq. (3) leads to $F(V,\tau)\le V^2F(1,\tau)$, so $\tilde{F}_V=V^2\mathcal{F}$ is the best possible scaling of the FI with V. This is a proof that for $V<1$ the HOM can never reach the QCR bound, even in the absence of losses. In addition, using (3) we see that the best possible scaling is obtained when $W(0,\tau_M)=0$ (i.e., $P_c(\tau_M)=1/2$) and $W'(0,\tau_M)\neq 0$. A sinusoidal function of frequency $\sqrt{\mathcal{F}}$ satisfies these conditions (a solution also leading to a constant FI in τ for $V=1$ [26,51]). This unphysical solution represents the limit situation of states occupying a large effective area in TFPS [52], as Schrödinger-cat-like (SC-like) states [18,20,53] with $\Delta^2\hat{\omega}_-\Delta^2\hat{t}\gg 1$ [26]. Surprisingly, SC-like states exhibit remarkable robustness in the presence of decreased visibility, making them the most resilient states in HOM-based quantum metrology, which is yet another interesting quality of these states in quantum metrology [54].

States leading to the worst possible scaling of $\tilde{F}_V$ with V minimize $\tilde{F}_{V<1}\ \forall\ V$. The quantity $-W''(0,\tau)$ in the region $\tau\ll\Delta\hat{\omega}_-$ is minimized by Gaussian states [55,56]. Consequently, in this region (where lies the value of the parameter to be estimated), Gaussian states also minimize $W'(0,\tau)$, so $W(0,\tau)$ is maximal. For this reason, they are the states exhibiting the worst scaling of $\tilde{F}_{V<1}$ with V, even when they have the same limit value for the FI as SC-like states for $V=1$ and $\tau=0$, i.e., the QFI. Interestingly, their scaling with V does not depend on the values of $\Delta\hat{\omega}_-$ or $\Delta\hat{t}$, but on the associated function (Gaussian), which is univocally determined by the product of the two quantities. As states' phase space occupation change from the Gaussian to the sinusoidal behavior, their scaling with visibility improves. Interestingly, while the wave function shape *does not* play a role in the value of $\mathcal{F}$ [26,45] it does play a role in the scaling of $\tilde{F}_V$ with V, in a way that is related to the effective occupation of the TFPS. Previous works [52] established the connection between metrological properties and the state's occupation of the quadrature phase space [57,58], where small structures determine quantum properties such as the QFI. Our analysis indicates that such structures also contribute to the optimization of the scaling of precision with visibility. We emphasize that our analysis is applicable to various experimental setups where the model (2) holds [33,34], such as experiments with more than two photons [59], where the scaling with V is important to determine the tolerance of the sub-shot-noise region to visibility decrease (see Refs. [26,33]).

TABLE I. f_- and $W(0,\tau)$ functions corresponding to the four states studied. The different variables introduced are defined in the left column of Fig. 2.

State	$f_-(\omega_-)$	$W(0,\tau)$
Sinc	$\mathrm{sinc}(a\omega_-^2 + b\omega_- + c)$	$\int d\omega_- f_-(\omega_-) f_-^*(-\omega_-) e^{-i\omega_-\tau}$
Gauss	$\exp(-\omega_-^2/2\sigma_{\omega_-}^2)$	$\exp(-\tau^2\sigma_{\omega_-}^2/2)$
Rect	$\Pi(\omega_-/\Delta\omega_-)$	$\mathrm{sinc}(\Delta\omega_-\tau/2)$
SC	$\Pi[(\omega_- - \omega')/\Delta\omega'] + \Pi[(\omega_- + \omega')/\Delta\omega']$	$\mathrm{sinc}(\Delta\omega'\tau/2)\cos(\omega'\tau)$

We now validate our model using an experiment allowing to engineer two-photon states described by different functions $f_-(\omega_-)$ exhibiting diverse scaling behaviors with the visibility V. The quantum source consists of an AlGaAs Bragg reflector waveguide, generating polarization-entangled photon pairs via type II spontaneous parametric down-conversion at telecom wavelengths and operating at room temperatures [60]. A sketch of the experimental setup is provided in Fig. 1. A continuous-wave laser having a wavelength $\lambda_{\mathrm{pump}} = 772.42$ nm is coupled into the waveguide using a microscope objective. The output signal is collected by a second microscope objective, and the pump beam is filtered out using a long-pass filter. The generated photon pairs are then collected in a single mode fiber and possibly directed to a programmable filter (Finisar 4000 s), enabling the JSA engineering. When the filter is not inserted, the state generated by the source is described by $f_-(\omega_-) = \mathrm{sinc}(a\omega_-^2 + b\omega_- + c)$ where the coefficients a, b, and c are related to optical properties of the material such as birefringence and chromatic dispersion [26,28].

In addition to the study of this case, three different filter shapes are used: a 15 nm-wide rectangular filter centered on the degeneracy wavelength $\lambda_{\mathrm{deg}} = 1544.8$ nm, a Gaussian filter of identical width centered at the same wavelength, and a combination of two 5 nm-wide rectangular filters centered at $\lambda_1 = 1560$ nm and $\lambda_2 = 1530$ nm corresponding to energy-matched channels and allowing to create a SC-like state, analogously to as described in [61,62]. The functions f_- and $W(0,\tau)$ associated with the four states are presented in Table I. They can be classified according to the parameter $\mathcal{S} = \Delta^2\hat{\omega}_-\Delta^2\hat{t}$, which determines the scaling with respect to V (see Ref. [26] for details).

At the output of the filtering process, the photon pairs are separated by a polarizing beam splitter (PBS). The H (V) polarized photon enters the HOM interferometer through the arm 1 (2). Precise control over the polarization distinguishability, and thus the HOM visibility, is enabled by two fibered polarization controllers, one in each arm (FPC1 and FPC2). The temporal delay between the two photons is controlled by a motorized optical delay line (MDL). The two paths are recombined and separated by a 50/50 BS, then directed to superconducting nanowires single photon detectors (SNSPD). Temporal correlations between the detected photons are analyzed by a time-to-digital converter (TDC).

We perform a series of measurements on the four states, systematically varying V to investigate the scaling of the ratio $\tilde{F}_V/\mathcal{F}$. Figure 2 illustrates the results obtained. The coincidence counts data (red points) are fitted (red lines) using $P_c(\tau)$ of Eq. (2) and the theoretical expression of each wave function [26]. The FI $F(V,\tau)$ (blue lines) is then computed using Eq. (3). The error bars associated to the experimental points are estimated assuming Poissonian statistics.

First, we notice that a reduction in visibility leads to a decrease in $F(V,\tau)$. As expected, with finite visibility, the value of $F(V,\tau)$ drops to zero at $\tau = 0$. Remarkably high visibilities exceeding 99% are achieved with the Gaussian, rectangular, and SC-like states. Because of a small modal birefringence of the AlGaAs source, the maximum visibility attainable with the full state is 94,9%, still an excellent

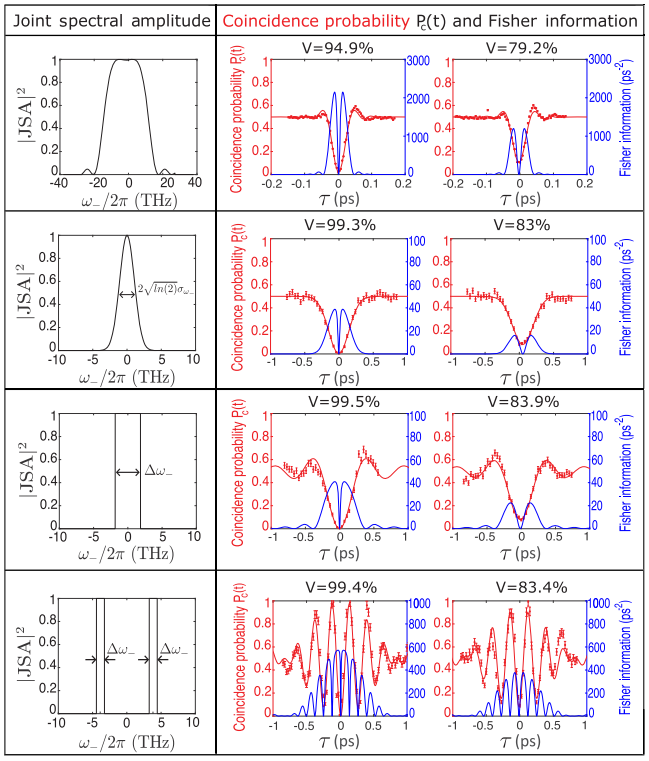

FIG. 2. Left column: Joint spectral amplitude of the four different states analyzed in this Letter. Central and right columns: corresponding Hong-Ou-Mandel coincidence probability $P_c(t)$ and FI for different values of visibility V.

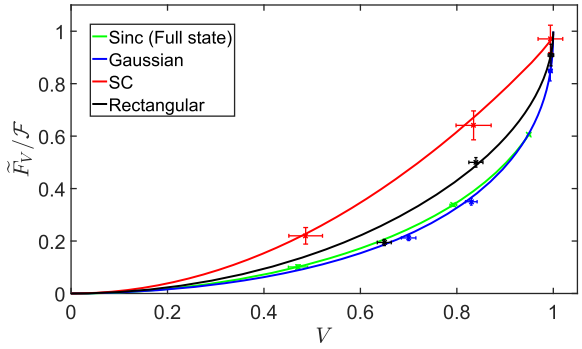

FIG. 3. Scaling of the ratio $\tilde{F}_V/\mathcal{F}$ for different biphoton states with respect to the HOM visibility V. For SC-like states a maximal value of $\tilde{F}_V/\mathcal{F} = 0.97$ is attained for $V = 99.4\%$. Notice that the experimental values of $\mathcal{F}$ are different for each state.

value given the broad spectral width it covers, ≈100 nm. This broad spectrum results in a narrow HOM curve $P_c(t)$, leading to a high FI value of 2100 ps^{-2}, which is 2 orders of magnitude higher than those obtained with the Gaussian and rectangular states. Filtering the quantum state decreases the number of detected photons, therefore influencing the overall performance of the metrological protocol in a given integration time. Nevertheless, in this proof-of-principle experiment, we are mainly interested in testing the scaling of the ratio $\tilde{F}_V/\mathcal{F} = \max_\tau F(V,\tau)/\Delta^2\omega_-$ to demonstrate our model, which can serve as a guideline to other experiments using different strategies. In Fig. 3, the evolution of this ratio with respect to visibility for the four engineered states is reported, both for experiments (points) and theory (lines). The error bars associated to the experimental points are estimated by extracting the visibility from the HOM interferogram fit reported in Fig. 2. The theoretical plots are obtained by using the functions f_- and $W(0,\tau)$ defined in Table I. We clearly observe that the SC-like state exhibits the most favorable scaling behavior, in contrast to the Gaussian state, which displays a less optimal one. For instance, at a visibility level of around 99.4% (83%), the ratio drops to 0.97 (0.64) for the SC-like state and to 0.85 (0.35) for the Gaussian state.

In conclusion, we have presented a well-grounded theoretical model and experimentally confirmed it, showing how precision limits scale with both visibility and the state's wave function in practical metrological protocols employing the HOM effect in the broadly used regime of time unresolved measurement. The very good agreement between the experimental results and the simulations supports the validity of the model given by Eq. (2). Our findings show that reaching the precision limits in realistic conditions presents challenges that depend on the particular state under consideration. Moreover, our theoretical and experimental analysis establishes a general framework for interpreting previous experimental results [17–20,63]. We focused on the time unresolved measurement regime rather in the time resolved measurements one, or other measurement strategies based on modal filtering or post-selection [61,63–66] because the latter do not depend on the initial wave function [62]. However, the obtained filtered modes will obey the same behavior as the one detailed in the present work, so these settings can also benefit from our results. Our Letter holds significant implications, particularly in aiding the identification of optimal conditions to advance HOM-based quantum metrology protocols, leading to enhanced precision in measurements while minimizing the number of repetitions. Finally, some aspects of the presented results can be readily extended to other experiments where parity measurements are employed for quantum parameter estimation [6,67–70].

We acknowledge funding from the Plan France 2030 through the Project No. ANR-22-PETQ-0006, N. Fabre, G. Bié Alves and J. Lorgeré for fruitful discussions, and M. Karr-Ducci for Fig. 1. O. M. acknowledges Labex SEAM (Science and Engineering for Advanced Materials and devices), ANR-10-LABX-0096 and ANR-18-IDEX-0001, for financial support.

*These authors contributed equally to this work.
†Corresponding author: sara.ducci@u-paris.fr
‡Corresponding author: perola.milman@u-paris.fr

[1] C. K. Hong, Z. Y. Ou, and L. Mandel, Measurement of subpicosecond time intervals between two photons by interference, Phys. Rev. Lett. **59**, 2044 (1987).
[2] N. Fabre, M. Amanti, F. Baboux, A. Keller, S. Ducci, and P. Milman, The Hong-Ou-Mandel experiment: From photon indistinguishability to continuous-variable quantum computing, Eur. Phys. J. D **76**, 196 (2022).
[3] B. Brecht and C. Silberhorn, Characterizing entanglement in pulsed parametric down-conversion using chronocyclic Wigner functions, Phys. Rev. A **87**, 053810 (2013).
[4] A. Eckstein and C. Silberhorn, Broadband frequency mode entanglement in waveguided parametric downconversion, Opt. Lett. **33**, 1825 (2008).
[5] M. R. Ray and S. J. van Enk, Verifying entanglement in the Hong-Ou-Mandel dip, Phys. Rev. A **83**, 042318 (2011).
[6] T. Douce, A. Eckstein, S. P. Walborn, A. Z. Khoury, S. Ducci, A. Keller, T. Coudreau, and P. Milman, Direct measurement of the biphoton Wigner function through two-photon interference, Sci. Rep. **3**, 3530 (2013).
[7] N. Tischler, A. Büse, L. G. Helt, M. L. Juan, N. Piro, J. Ghosh, M. J. Steel, and G. Molina-Terriza, Measurement and shaping of biphoton spectral wave functions, Phys. Rev. Lett. **115**, 193602 (2015).
[8] S. Kurzyna, M. Jastrzebski, N. Fabre, W. Wasilewski, M. Lipka, and M. Parniak, Variable electro-optic shearing interferometry for ultrafast single-photon-level pulse characterization, Opt. Express **30**, 39826 (2022).
[9] S. Francesconi, A. Raymond, N. Fabre, A. Lemaître, M. I. Amanti, P. Milman, F. Baboux, and S. Ducci, Anyonic two-photon statistics with a semiconductor chip, ACS Photonics **8**, 2764 (2021).

[10] S. Francesconi, F. Baboux, A. Raymond, N. Fabre, G. Boucher, A. Lemaître, P. Milman, M. I. Amanti, and S. Ducci, Engineering two-photon wavefunction and exchange statistics in a semiconductor chip, Optica **7**, 316 (2020).
[11] K. Dorfman, S. Asban, B. Gu, and S. Mukamel, Hong-Ou-Mandel interferometry and spectroscopy using entangled photons, Commun. Phys. **4**, 49 (2021).
[12] B. Ndagano, H. Defienne, D. Branford, Y. Shah, A. Lyons, N. Westerberg, E. M. Gauger, and D. Faccio, Quantum microscopy based on Hong–Ou–Mandel interference, Commun. Phys. **16**, 384 (2022).
[13] S.-Y. Lee and H. Nha, Second-order superposition operations via Hong-Ou-Mandel interference, Phys. Rev. A **85**, 043816 (2012).
[14] E. Descamps, A. Keller, and P. Milman, Time-frequency metrology with two single-photon states: Phase-space picture and the Hong-Ou-Mandel interferometer, Phys. Rev. A **108**, 013707 (2023).
[15] N. Fabre and S. Felicetti, Parameter estimation of time and frequency shifts with generalized Hong-Ou-Mandel interferometry, Phys. Rev. A **104**, 022208 (2021).
[16] K. M. Jordan, R. A. Abrahao, and J. S. Lundeen, Quantum metrology timing limits of the Hong-Ou-Mandel interferometer and of general two-photon measurements, Phys. Rev. A **106**, 063715 (2022).
[17] A. Lyons, G. C. Knee, E. Bolduc, T. Roger, J. Leach, E. M. Gauger, and D. Faccio, Attosecond-resolution Hong-Ou-Mandel interferometry, Sci. Adv. **4**, eaap9416 (2018).
[18] Y. Chen, M. Fink, F. Steinlechner, J. P. Torres, and R. Ursin, Hong-Ou-Mandel interferometry on a biphoton beat note, npj Quantum Inf. **5**, 43 (2019).
[19] C. Chen, Y. Chen, and L. Chen, Spectrally resolved Hong-Ou-Mandel interferometry with discrete color entanglement, Phys. Rev. Appl. **19**, 054092 (2023).
[20] S. J. Johnson, C. P. Lualdi, A. P. Conrad, N. T. Arnold, M. Vayninger, and P. G. Kwiat, Toward vibration measurement via frequency-entangled two-photon interferometry, in *Quantum Sensing, Imaging, and Precision Metrology*, edited by J. Scheuer and S. M. Shahriar, International Society for Optics and Photonics (SPIE, 2023), Vol. 12447, p. 124471C, 10.1117/12.2650820.
[21] H. Scott, D. Branford, N. Westerberg, J. Leach, and E. M. Gauger, Beyond coincidence in Hong-Ou-Mandel interferometry, Phys. Rev. A **102**, 033714 (2020).
[22] M. A. Taylor and W. P. Bowen, Quantum metrology and its application in biology, Phys. Rep. **615**, 1 (2016).
[23] A. M. Steinberg, P. G. Kwiat, and R. Y. Chiao, Dispersion cancellation and high-resolution time measurements in a fourth-order optical interferometer, Phys. Rev. A **45**, 6659 (1992).
[24] H. Scott, D. Branford, N. Westerberg, J. Leach, and E. M. Gauger, Noise limits on two-photon interferometric sensing, Phys. Rev. A **104**, 053704 (2021).
[25] C. Torre, A. McMillan, J. Monroy-Ruz, and J. C. F. Matthews, Sub-μm axial precision depth imaging with entangled two-color Hong-Ou-Mandel microscopy, Phys. Rev. A **108**, 023726 (2023).
[26] See Supplemental Material at http://link.aps.org/supplemental/10.1103/PhysRevLett.132.193603, which includes Refs. [27–32], for details of the calculations and extra figures.
[27] M. Jachura, R. Chrapkiewicz, R. Demkowicz-Dobrzański, W. Wasilewski, and K. Banaszek, Mode engineering for realistic quantum-enhanced interferometry, Nat. Commun. **7**, 11411 (2016).
[28] G. Maltese, Generation and manipulation of high-dimensional photonics states with AlGaAs chips, Ph.D. thesis, thèse de doctorat dirigée par Ducci, Sara Physique, Optique Quantique Sorbonne Paris Cité, 2019.
[29] F. Graffitti, P. Barrow, A. Pickston, A. M. Brańczyk, and A. Fedrizzi, Direct generation of tailored pulse-mode entanglement, Phys. Rev. Lett. **124**, 053603 (2020).
[30] G. Boucher, T. Douce, D. Bresteau, S. P. Walborn, A. Keller, T. Coudreau, S. Ducci, and P. Milman, Toolbox for continuous variable entanglement production and measurement using spontaneous parametric down conversion, Phys. Rev. A **92**, 023804 (2015).
[31] T. Yamazaki, T. Arizono, T. Kobayashi, R. Ikuta, and T. Yamamoto, Linear optical quantum computation with frequency-comb qubits and passive devices, Phys. Rev. Lett. **130**, 200602 (2023).
[32] A. F. Abouraddy, M. B. Nasr, B. E. A. Saleh, A. V. Sergienko, and M. C. Teich, Quantum-optical coherence tomography with dispersion cancellation, Phys. Rev. A **65**, 053817 (2002).
[33] M. Penasa, S. Gerlich, T. Rybarczyk, V. Métillon, M. Brune, J. M. Raimond, S. Haroche, L. Davidovich, and I. Dotsenko, Measurement of a microwave field amplitude beyond the standard quantum limit, Phys. Rev. A **94**, 022313 (2016).
[34] D. A. R. Dalvit, R. L. de Matos Filho, and F. Toscano, Quantum metrology at the Heisenberg limit with ion trap motional compass states, New J. Phys. **8**, 276 (2006).
[35] V. Giovannetti, S. Lloyd, and L. Maccone, Quantum metrology, Phys. Rev. Lett. **96**, 010401 (2006).
[36] S. Boixo, S. T. Flammia, C. M. Caves, and J. M. Geremia, Generalized limits for single-parameter quantum estimation, Phys. Rev. Lett. **98**, 090401 (2007).
[37] H. Cramer, *Mathematical Methods of Statistics* (Princeton University Press, Princeton, NJ, 1946), pp. xvi, 575.
[38] M. Jarzyna and R. Demkowicz-Dobrzański, True precision limits in quantum metrology, New J. Phys. **17**, 013010 (2015).
[39] O. Pinel, J. Fade, D. Braun, P. Jian, N. Treps, and C. Fabre, Ultimate sensitivity of precision measurements with Gaussian quantum light: A multi-modal approach, Phys. Rev. A **85**, 010101(R) (2012).
[40] M. Gessner, N. Treps, and C. Fabre, Quantum limits on mode parameter estimation, Optica **10**, 996 (2023).
[41] H. F. Hofmann, All path-symmetric pure states achieve their maximal phase sensitivity in conventional two-path interferometry, Phys. Rev. A **79**, 033822 (2009).
[42] K. P. Seshadreesan, S. Kim, J. P. Dowling, and H. Lee, Phase estimation at the quantum Cramér-Rao bound via parity detection, Phys. Rev. A **87**, 043833 (2013).
[43] In some situations, $P_a(\tau)$ can be directly measured, as in the case of [20] where an entangled state of non-degenerate photons is used as a probe.

[44] V. Giovannetti, S. Lloyd, and L. Maccone, Quantum-enhanced positioning and clock synchronization, Nature (London) **412**, 417 (2001).
[45] E. Descamps, N. Fabre, A. Keller, and P. Milman, Quantum metrology using time-frequency as quantum continuous variables: Resources, sub-shot-noise precision and phase space representation, Phys. Rev. Lett. **131**, 030801 (2023).
[46] We could have chosen it to be an odd function as well, and in the discussion that follows we would work with an antisymmetric function rather than a symmetric one.
[47] B. Escher, R. de Matos Filho, and L. Davidovich, General framework for estimating the ultimate precision limit in noisy quantum-enhanced metrology, Nat. Phys. **7**, 406 (2001).
[48] Y. L. Len, T. Gefen, A. Retzker, and J. Kołodyński, Quantum metrology with imperfect measurements, Nat. Commun. **13**, 6971 (2022).
[49] M. Fadel and L. Maccone, Time-energy uncertainty relation for quantum events, Phys. Rev. A **104**, L050204 (2021).
[50] N. Fabre, A. Keller, and P. Milman, Time and frequency as quantum continuous variables, Phys. Rev. A **105**, 052429 (2022).
[51] C. Cafaro and P. M. Alsing, Decrease of Fisher information and the information geometry of evolution equations for quantum mechanical probability amplitudes, Phys. Rev. E **97**, 042110 (2018).
[52] W. H. Zurek, Sub-Planck structure in phase space and its relevance for quantum decoherence, Nature (London) **412**, 712 (2001).
[53] S. Ramelow, L. Ratschbacher, A. Fedrizzi, N. K. Langford, and A. Zeilinger, Discrete tunable color entanglement, Phys. Rev. Lett. **103**, 253601 (2009).
[54] Entangled non-degenerate photons are also useful to produce broadband states in the collective variable ω_- using single photons with relatively narrow spectrum (before being entangled with one another).
[55] P. P. Rohde, T. C. Ralph, and M. A. Nielsen, Optimal photons for quantum-information processing, Phys. Rev. A **72**, 052332 (2005).
[56] F. Töppel, A. Aiello, and G. Leuchs, All photons are equal but some photons are more equal than others, New J. Phys. **14**, 093051 (2012).
[57] H. Kwon, K. C. Tan, T. Volkoff, and H. Jeong, Nonclassicality as a quantifiable resource for quantum metrology, Phys. Rev. Lett. **122**, 040503 (2019).
[58] B. Yadin, F. C. Binder, J. Thompson, V. Narasimhachar, M. Gu, and M. S. Kim, Operational resource theory of continuous-variable nonclassicality, Phys. Rev. X **8**, 041038 (2018).
[59] Z. Y. Ou, Multi-photon interference and temporal distinguishability of photons, Int. J. Mod. Phys. B **21**, 5033 (2007).
[60] F. Appas, O. Meskine, A. Lemaître, M. Morassi, F. Baboux, M. I. Amanti, and S. Ducci, Nonlinear quantum photonics with AlGaAs Bragg-reflection waveguides, J. Lightwave Technol. **40**, 7658 (2022).
[61] Z. Y. Ou and L. Mandel, Observation of spatial quantum beating with separated photodetectors, Phys. Rev. Lett. **61**, 54 (1988).
[62] N. Fabre, J. Belhassen, A. Minneci, S. Felicetti, A. Keller, M. I. Amanti, F. Baboux, T. Coudreau, S. Ducci, and P. Milman, Producing a delocalized frequency-time Schrödinger-cat-like state with Hong-Ou-Mandel interferometry, Phys. Rev. A **102**, 023710 (2020).
[63] D. Triggiani, G. Psaroudis, and V. Tamma, Ultimate quantum sensitivity in the estimation of the delay between two interfering photons through frequency-resolving sampling, Phys. Rev. Appl. **19**, 044068 (2023).
[64] J. M. Donohue, V. Ansari, J. Řeháček, Z. Hradil, B. Stoklasa, M. Paúr, L. L. Sánchez-Soto, and C. Silberhorn, Quantum-limited time-frequency estimation through mode-selective photon measurement, Phys. Rev. Lett. **121**, 090501 (2018).
[65] H. Scott, D. Branford, N. Westerberg, J. Leach, and E. M. Gauger, Beyond coincidence in Hong-Ou-Mandel interferometry, Phys. Rev. A **102**, 033714 (2020).
[66] C. Chen, Y. Chen, and L. Chen, Spectrally resolved Hong-Ou-Mandel interferometry with discrete color entanglement, Phys. Rev. Appl. **19**, 054092 (2023).
[67] L. G. Lutterbach and L. Davidovich, Method for direct measurement of the Wigner function in cavity QED and ion traps, Phys. Rev. Lett. **78**, 2547 (1997).
[68] P. Bertet, A. Auffeves, P. Maioli, S. Osnaghi, T. Meunier, M. Brune, J. M. Raimond, and S. Haroche, Direct measurement of the Wigner function of a one-photon fock state in a cavity, Phys. Rev. Lett. **89**, 200402 (2002).
[69] Y. Shalibo, R. Resh, O. Fogel, D. Shwa, R. Bialczak, J. M. Martinis, and N. Katz, Direct Wigner tomography of a superconducting anharmonic oscillator, Phys. Rev. Lett. **110**, 100404 (2013).
[70] F.-R. Winkelmann, C. A. Weidner, G. Ramola, W. Alt, D. Meschede, and A. Alberti, Direct measurement of the Wigner function of atoms in an optical trap, J. Phys. B **55**, 194004 (2022).